RSC Advances

PAPER

View Article Online
View Journal | View Issue

Cite this: *RSC Adv.*, 2017, **7**, 52345

One-pot hydrothermal synthesis and selective etching method of a porous $MoSe_2$ sand rose-like structure for electrocatalytic hydrogen evolution reaction†

Xuan Thai Tran, Sujittra Poorahong and Mohamed Siaj *

The development of a platinum-free electrocatalyst for the hydrogen evolution reaction (HER) is highly essential to the large-scale production and application of water splitting devices. Herein we report a facile one-pot hydrothermal synthesis of composite $MoSe_2$@Cu_2Se. The morphology of the obtained material was characterized by scanning electron microscope (SEM) and it was found that the composite material formed a sand rose-like structure. The crystal structure and phase purity of the composite $MoSe_2$@Cu_2Se were investigated by X-ray diffraction (XRD) and transmission electron microscopy (TEM). Then a selective electrochemical etching of copper from the composite was carried out and the porous $MoSe_2$ rose-like nanosphere was obtained. The robust 3D $MoSe_2$ rose-like structure exhibit remarkable activity and durability for electrocatalytic HER in acid maintaining a small onset overpotential of ~150 mV and keeping a small overpotential of 300 mV for 6 mA cm^{-2} current density after 1000 cycles. Based on our data, the obtained porous sand rose-like structure material could improve the active surface area which yields higher HER catalytic activity. The present study provides a simple and effective way for the exploration of efficient Mo-based HER catalysts.

Received 7th September 2017
Accepted 26th October 2017

DOI: 10.1039/c7ra10001a

rsc.li/rsc-advances

Introduction

Hydrogen (H_2) is a promising, clean, and renewable energy carrier to relieve our reliance on natural fossil fuels and can reduce the growing global greenhouse effects.[1–3] Growing attention has been paid to the sustainable hydrogen evolution reaction (HER) from the water splitting reaction, which is a clean and environmentally benign reaction pathway.[3,4] The most effective electrocatalyst for the HER in an acidic media is Pt group metals. However, several challenges remain in designing and selecting an electrocatalyst material. These are related to the expensiveness of Pt and low earth-abundance, which hinder its practical implementation.[5,6] Limited surface active sites impede the HER from proceeding efficiently[7] and chemical and structural stability issues of electrocatalysts in a harsh acidic environment were also another problem.[8] These limitations have motivated several researchers to dedicate intensive efforts in designing and fabricating low-cost and plentiful HER electrocatalysts with high catalytic activities.[9]

In recent years, many alternatives for non-precious metal-based electrocatalysts have been developed, including transition metal sulfides, selenides, borides, carbides, nitrides, phosphides, and a molecular catalyst family. Among all these alternatives a type of efficient electrocatalysts based on transition metal dichalcogenide (TMD) has recently received significant attention, because of its exotic electronic structure and these physical properties.[10] TMD is a family of materials consisting of more than 40 compounds having the generalized formula MX_2, wherein M is a transition metal, typically 4–7 groups and X is a chalcogen such as sulfur (S), selenium (Se) and tellurium (Te). These transition metals have an important catalytic behavior in the HER. The latter trend has formed with superimposed layers of weak interactions of van der Waals between two adjacent layers,[10] this form has two large areas on the sides (active sites) for the adsorption of ions. It has been proven by further research that TMD slips active sites play an important role in HER. Among them, $MoSe_2$ is a newly emerging catalyst owing to its low cost, high chemical stability, and excellent electrocatalytic activity.[11–15] The electrocatalytic HER activity of $MoSe_2$ depends strongly on its active selenium edge sites, while its basal planes were catalytically inert.[16] In order to obtain, a high performance $MoSe_2$ electrocatalyst towards the HER is to rationally construct the nanostructure for mass transfer and maximizing the number of active sites. A boost of the catalytic activities could be achieved by reducing

Department of Chemistry and Biochemistry, Université du Quebec à Montréal, Montréal, QC, H3C 3P8, Canada. E-mail: siaj.mohamed@uqam.ca

† Electronic supplementary information (ESI) available: One-pot hydrothermal synthesis and selective etching method of porous $MoSe_2$ sand rose-like structure for electrocatalytic hydrogen evolution reaction. See DOI: 10.1039/c7ra10001a

the $MoSe_2$ crystal size to nanoscale level and by increasing the exposures of its active edges to the electrolytes. In one aspect, a high surface area with an open structure avail the diffusion of electrolytes, will lead smoothly to the replenishment of the consumed protons and lower the ohmic drop at high reaction rate.[17]

Herein, we demonstrate the preparation of a 3D hierarchical porous $MoSe_2$ by a combination of hydrothermal and chemical etching methods. To the best of our knowledge, here is the first report of the $MoSe_2$@Cu_2Se synthesis by hydrothermal method. After $MoSe_2$@Cu_2Se synthesis, the copper is selectively etched from the alloy leading to a 3D porous $MoSe_2$ structure formation (sand rose-like structure). The 3D porous $MoSe_2$ material is tested as a catalyst for HER. A comparison between pure $MoSe_2$ and porous $MoSe_2$ sand rose-like structure shows that the porous one exhibits higher catalytic activity for electrocatalytic HER.

Experimental

Synthesis porous $MoSe_2$

The preparation procedure of Mo@Cu selenide composite is schematically described in Fig. 1. The Synthesis was carried out using 0.42 g of ammonium molybdate tetrahydrate, 0.6 g copper(II) sulfate pentahydrate and 1.065 g SeO_2 powder in 20 mL of distilled water under vigorous stirring for 45 minutes to form a homogeneous solution. After that, 50 mL of ethylene diamine was added with stirring continuously for 15 min at room temperature. The final solution has given a greenish color. The solution was then transferred to a stainless-steel autoclave with 100 mL Teflon coated and maintained at 210 °C for 23 h; Fig. 1A. After the reaction, the system was cooled down to room temperature. The precipitated black obtained were collected by centrifugation at 4000 rpm for 15 minutes, washed with distilled water and ethanol at least 4 times, and then dried at 60 °C under vacuum. To yield the final crystalline products, the precipitate products were dried at 500 °C for 1 h in an atmosphere of argon (Ar). After that, the copper component was etched out from the composite under sonication in 0.5 M ammonium persulfate for 30 min. After the etching procedure, the porous $MoSe_2$ sand rose-like structure was obtained (Fig. 1B). As a control experiment, the synthesis of pure $MoSe_2$ and Cu_2Se were prepared following the same method motioned above.

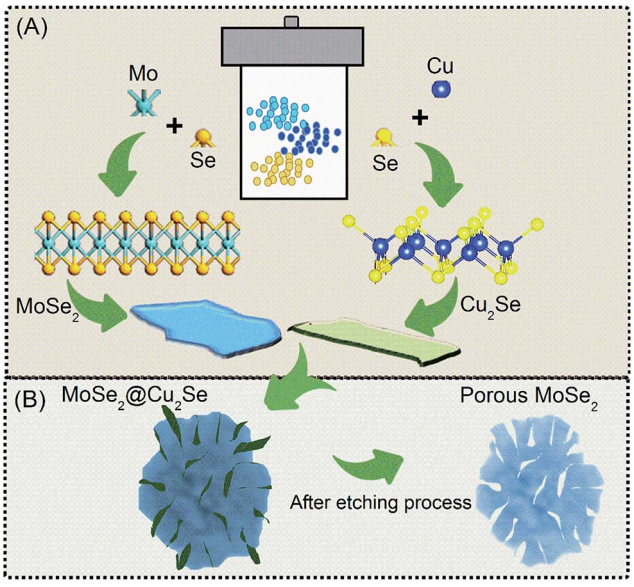

Fig. 1 (A) The procedure of the $MoSe_2$@Cu_2Se powder synthesis. (B) The expected morphology after etching process.

Electrochemical measurement

All electrochemical measurements were performed in a disposable three electrodes system (EP-PP, Biodevice Technology, Japan) consisted of a working electrode (carbon, 2 mm diameter), a counter electrode (carbon) and a reference electrode (Ag/AgCl). The electrochemical experiments were performed at room temperature and were carried out using SP-300 potentiostat (Bio-Logic Science Instrument, France) connected to a personal computer and driven by EC-Lab software. Prior to all electrochemical measurements, 60 mg of porous $MoSe_2$ product and 150 μL of Nafion solution (Sigma Aldrich, 5 wt%) was dispersed in a 5 mL water-ethanol solution with a volume ratio of 4 : 1 by at least 30 min sonication to from a homogeneous ink. Finally, 3 μL of as-prepared slurry (containing 35 μg of catalyst) was dropped on to the carbon-working electrode. Finally, the as-prepared catalyst film was dried in the air at room temperature.

Linear sweep voltammetry (LSV) was performed in 0.5 M H_2SO_4 saturated using an Ag/AgCl as the reference electrode, and a carbon as the counter electrode. All the potentials were calibrated to a reversible hydrogen electrode (RHE). LSV was recorded by sweeping the potential from 0.2 to −0.8 V *vs.* RHE with a scan rate of 1 mV s^{-1} at room temperature. Cyclic voltammetry (CV) was conducted for 1000 cycles between 0.1 V to −0.8 V (*vs.* RHE) at 100 mV s^{-1} for the stability test. The Nyquist plots were measured with frequencies ranging from 200 kHz to 100 mHz at an overpotential of −250 mV. The impedance data were then plotted to a simplified Randles circuit to extract the series and charge-transfer resistances.

Characterization

The X-ray diffraction (XRD) was performed using a diffractometer (Bruker D8 Advance) with Cu-Kα radiation ($\lambda = 1.54182$ Å) at room temperature. X-ray photoelectron spectroscopy (XPS) data for elemental composition and valence information was collected with XPS PHI 5600-ci (Physical Electronics, Eden Prairie, MN, USA). Scanning electron microscope was recorded on JEOL (JSM7600F) with an accelerating voltage of 10 kV and a working distance of 5 mm using secondary electron imaging mode. Raman spectra of the films were recorded with alpha300 R Confocal Raman Microscope with WITec UHTS 300 spectrometer with a 532 nm laser. Transmission electron microscopy (TEM) and Energy-dispersive X-ray spectroscopy (EDS) was performed on a Joel JEM-2100F.

Results and discussion

Structure and morphology of porous $MoSe_2$

The crystallographic structures and phase purity of as-prepared materials were determined by XRD. Fig. 2A-(i), shows the diffraction peaks in the two-theta range of 10–80° which implies the crystalline nature of the obtained materials. The asymmetric-shaped and broadening diffraction peaks, which are the typical features of 2D nanosheets, demonstrate that the $MoSe_2$ rose-like structure is completely comprised of layered flakes.[12] All of these diffraction peaks are in good agreement with the characteristic planes *i.e.*, (002), (100), (103) and (110) of the hexagonal $MoSe_2$ phase (JCPDS 29-0914), revealing the high purity of the as-synthesized product. In the case of copper selenide synthesis, Fig. 2A-(ii), the XRD patterns exhibit well-defined peaks which were indicated with the standard pattern of Cu_2Se (JCPDS no. 01-088-2043). Fig. 2A-(iii) shows the XRD pattern of the composite Mo@Cu selenide. It can be seen that all diffraction peaks in the $MoSe_2$@Cu_2Se composite the X-ray diffraction patterns can be separated from the compounds either $MoSe_2$ or Cu_2Se, demonstrating a phase purity of the synthesized product. In addition, the peaks compatible with those indicated by the virgin $MoSe_2$ are enlarged. These characteristics show that the Cu_2Se compound tends to aggregate and form larger sizes, while $MoSe_2$ retains its nanometric size distribution in the $MoSe_2$@Cu_2Se composite. After etching processes, the XRD pattern of Cu_2Se disappeared, showing only the pattern corresponding to $MoSe_2$ (Fig. 2A-(iv)). From the XRD result, it can be concluded that the Cu_2Se was successfully eliminated.

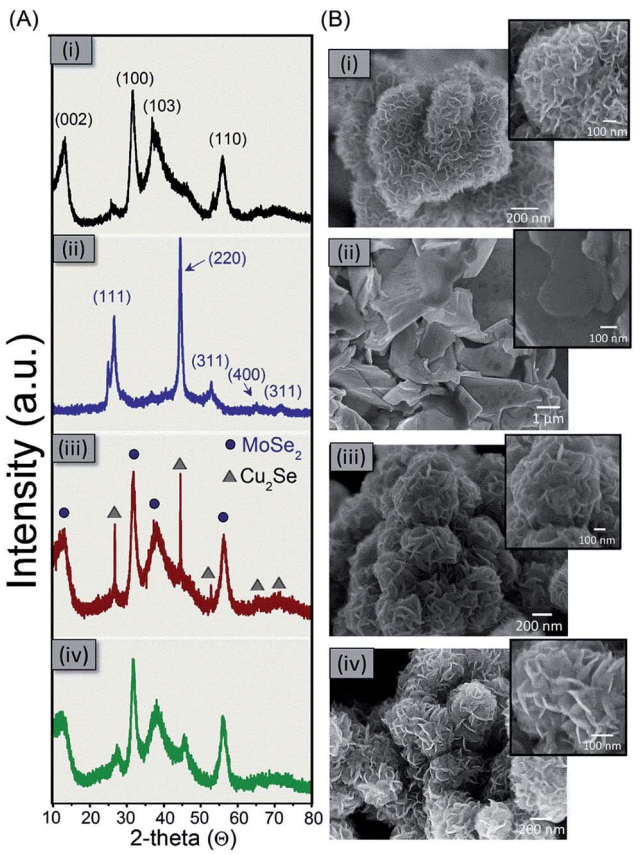

Fig. 2 (A) The XRD pattern and (B) the SEM morphology of the as-prepared materials grown by solvothermal method (i) $MoSe_2$, (ii) Cu_2Se, (iii) $MoSe_2$@Cu_2Se and (iv) porous $MoSe_2$ after etching the Cu_2Se.

Fig. 2B-(i) presents the morphology of pure $MoSe_2$ produced by the solvothermal process involving $(NH_4)_6Mo_7O_{24}\cdot 4H_2O$ as the Mo source and SeO_2 as the Se source. The morphology of pristine $MoSe_2$ can be described as the rose-like microsphere that consists of a large number of petals. While Cu_2Se has an irregular morphology in the form of dense nanoplates and/or nanocrystals, Fig. 2B-(ii). Even though pure $MoSe_2$ and composite $MoSe_2$@Cu_2Se have rose-like microsphere morphology, the petals of pure $MoSe_2$ are thinner than that from $MoSe_2$@Cu_2Se composite. Also, compared spaces between the petals of the material composite are denser than $MoSe_2$. Fig. 2B-(iv) shows SEM images indicate that after etching the composite of the rose-like structures remains intact with more porous and opened structure. Such enormous nanosheets could provide a large number of active sites accompanied with a large specific surface area. The dispersion homogeneity of the different components is supported by the selected element mapping of Mo, Cu and Se (ESI Fig. S1†). The mapping of $MoSe_2$@Cu_2Se composite sample demonstrates clearly the existence of each element, in addition to being well distributed over the composite material. After the etching process, no copper element was detected. This mapping confirms that the etching process has been done successfully.

The low-resolution TEM images in Fig. 3A and B indicate the rose-like structure formation of porous $MoSe_2$. High-resolution transmission electron microscopy (HRTEM) images of the $MoSe_2$ reveal the microscopic phase information as well as the thickness of the $MoSe_2$. It can be seen that each section of the nanoflowers presenting a shape of a petal is actually an individual stack of 2D $MoSe_2$ thin layers. A large amount of active sites can be attributed to widely distributed petals, which would offer much more active sites for HER. The spacing between two adjacent monolayers is 0.277 nm, which is consistent with the value of $MoSe_2$ interlayer spacing of the (100) plane (Fig. 3C). The selected area electron diffraction (SAED) results also reflect the (002) planes of 2H-$MoSe_2$ clearly in the inset Fig. 3C. Fig. 3D shows the other plane of $MoSe_2$ obtained from the average values for five layers is 0.72 nm, in good accordance with the thickness of the atomic layer of Se–Mo–Se unit where the *c*-axis orients normal to the (002) lattice plane. Therefore, we conclude that the $MoSe_2$ porous microspheres are composed of $MoSe_2$ monolayer flakes in an incompact way. Furthermore, the comparison between TEM images of pure $MoSe_2$ (ESI Fig. S2A†) and $MoSe_2$ after etching process (ESI Fig. S2B†), the pure $MoSe_2$ looks denser than those $MoSe_2$ after etching. On the other word, after took Cu_2Se out from composite material, $MoSe_2$ becomes hollow. To prove that the specific area increased indeed, Brunauer–Emmett–Teller (BET) method was used to measure the surface area of the pure and etched $MoSe_2$. ESI Fig. S3A† shows nitrogen adsorption and desorption isotherms for the porous $MoSe_2$ sample. It showed a hysteresis loop curve, which is the characteristic of a mesoporous material. BET specific surface

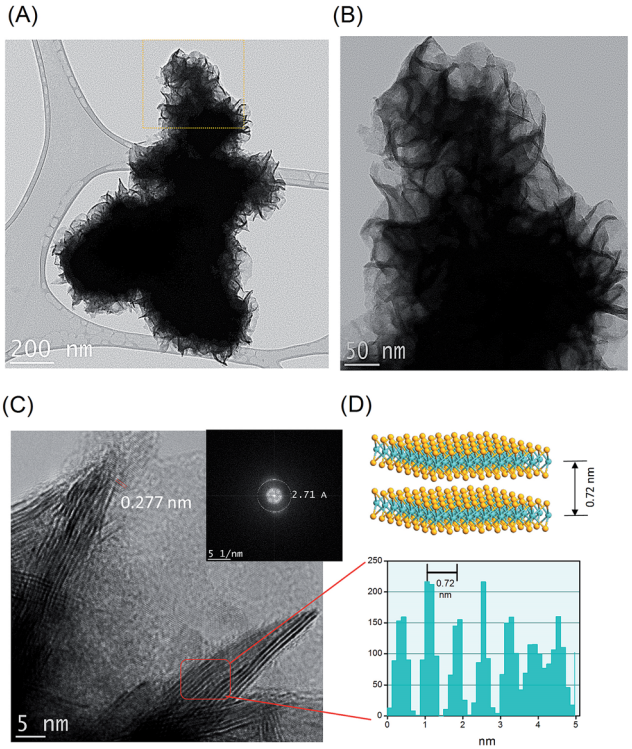

Fig. 3 (A and B) TEM images porous $MoSe_2$ under different magnifications. (C) HRTEM image of an area of the surface of $MoSe_2$; inset the selected area electron diffraction profile. (D) Plot of the calibration for measuring the spacing and the corresponding atomic stacking models.

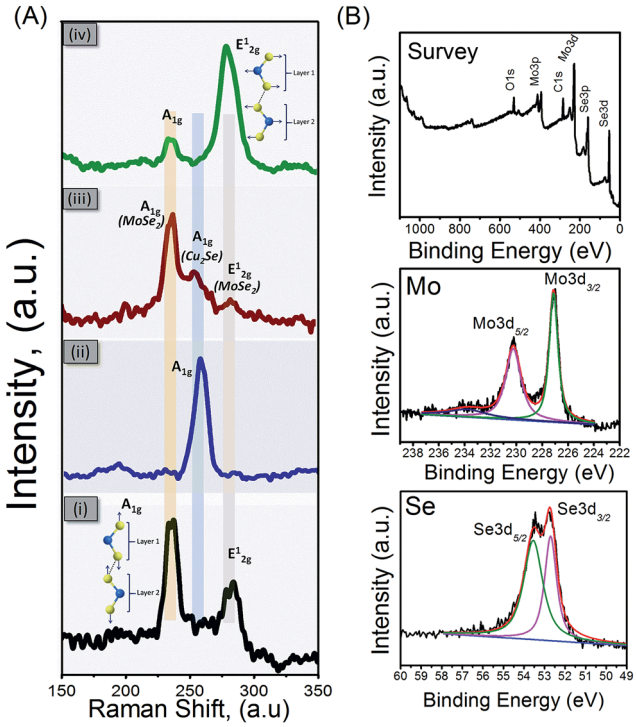

Fig. 4 (A) Raman spectra of (i) $MoSe_2$, (ii) Cu_2Se , (iii)$MoSe_2$@Cu_2Se and (iv) porous $MoSe_2$ after etched Cu_2Se; inset the atomic vibration manners of the A^1_g and E^1_{2g} vibrational modes of $MoSe_2$. Blue and yellow balls represent Mo and Se atoms, respectively. (B) XPS survey and high-resolution spectra showing the binding energies of Mo 3d and Se 3d of porous $MoSe_2$.

area for the porous $MoSe_2$ sample was 33.59 $m^2\ g^{-1}$ while that the porous $MoSe_2$ was only 12.31 $m^2\ g^{-1}$. So, the surface area of the composite increased by about 2.72 times compared with pure $MoSe_2$. Then the density functional theory (DFT) was applied to calculate the pore size distribution from the adsorption isotherm. As you can see in ESI Fig. S3B,† the material possesses the micropores characteristic from the range of 23–54 Å. It has been expected that the relatively large surface area of the as-prepared porous $MoSe_2$ rose-like microspheres not only can provide more active sites but also enhance the conductivity, which may improve the performance for a further application.

Then the Raman spectroscopy of all samples has been carried out. The observation of the Raman spectra of $MoSe_2$ (Fig. 4A-(i)) can be noted that there are two resonance peaks at 238 cm^{-1} and 283 cm^{-1} which can be well indexed to the out-of-plane A_{1g} and in-plane E^1_{2g} modes of 2H-$MoSe_2$, respectively.[18] In the Cu_2Se Raman spectrum (Fig. 4A-(ii)), an active mode A_{1g} at 257 cm^{-1} is observed. It is corresponding to Cu–Se vibration and is in good agreement with the literature.[19] In the Raman spectrum of $MoSe_2$@Cu_2Se composite (Fig. 4A-(iii)), it can be noted that the two-mode vibration at 237 cm^{-1} $MoSe_2$ and at 256 cm^{-1} Cu_2Se appears in this spectrum. After the etching process (Fig. 4A-(iv)), the sample exhibits two Raman peak at 237.1 cm^{-1} and 283.1 cm^{-1}. In addition, as can be seen, the A_{1g} peak intensity is much higher than the E^1_{2g} peak at pure $MoSe_2$ and $MoSe_2$ composite. This Raman peak corresponding to the out-of-plane Mo–Se phonon mode is preferentially excited for the edge-terminated perpendicularly-oriented nanosheets.[11] Moreover, after etching process, the E^1_{2g} peak intensity is much higher than A_{1g} peak where the E^1_{2g} peak is preferentially excited for terrace-terminated film. It can be supported the porous structure $MoSe_2$ formation. These make a relatively weak layer–layer interactions in the porous $MoSe_2$ nanosheets happen and in-plan Mo–Se phonon occurs. Photoluminescence spectroscopy was used to investigate the optical emission properties of porous $MoSe_2$. As shown in ESI Fig. S4† the porous $MoSe_2$ shows bandgap energy of 1.54 eV.

Chemical compositions on the surface and valence states of the porous $MoSe_2$ rose-like microspheres were further investigated by X-ray photoelectron spectroscopy (XPS) measurements. Fig. 4B shows the XPS survey spectrum of $MoSe_2$ after etched Cu_2Se out. In which the peaks derived from Mo, Se, C and O elements were detected; no Cu peak was observed compared to composite materials sample (ESI Fig. S5†). Generally, a small amount of oxygen may be due to surface adsorption of oxygen, and the C 1s peak located at 284.6 eV mainly results from the contamination from the used carbon conductive tabs. The core-level XPS spectra of Mo 3d shows the binding energies at 229 eV and 232.1 eV belong to Mo $3d_{5/2}$ and $3d_{3/2}$ spin orbit peaks of $MoSe_2$, confirming the elemental chemical state of Mo is mainly the Mo^{4+} oxidation state in the hexagonal 2H phase of $MoSe_2$. In

case of Se, two fitted peaks at 55.4 and 54.5 eV attributable to the core levels of Se $3d_{3/2}$ and Se $3d_{5/2}$, respectively, are further illustrating Se^{2-} of the $MoSe_2$.

All of the above characterization results prove that the hybrid $MoSe_2$@$CuSe_2$ is the individual compound and formation can be described as followed. Under the solvothermal condition, as the temperature and pressure increase, Mo(VI) reduced to Mo(IV) by $C_2H_8N_2$ and then reacts with Se from the decomposition of SeO_2 to form $MoSe_2$. At the same time, the Cu_2Se nanoparticles also form *via* stacking of a redox reaction occurred between the copper and the Se_x^{2-} to form Cu_2Se crystal.[19] The generated $MoSe_2$ and Cu_2Se nucleus accumulates and leads to nanosheets growth. With the increasing time, the nanosheets of both materials tend to aggregate to form 2D layer and several layers stack under the influence of the hydrogen bonding interaction and thermodynamic stability[20] and finally formed 3D hierarchical microsphere-like of composite $MoSe_2$@Cu_2Se. As resulting in the elements are well distributed over the composite material. Furthermore, the etching process does not inhibit the $MoSe_2$ properties.

Electrocatalytic analysis

The as-prepared porous $MoSe_2$ rose-like microspheres combine the advantages of the intrinsic properties of 2D $MoSe_2$ monolayer flakes and the 3D porous structures, which are believed to greatly benefit their applications. Here, we investigate their electrocatalytic activity for HER in acid. HER is the key process to electrolytic or photoelectrochemical water splitting. The search for efficient and robust HER electrocatalysts is at the heart of clean energy research. To investigate the HER performance of the synthesized porous $MoSe_2$, the electrochemical measurements were carried out in a N_2-saturated 0.5 M H_2SO_4 at room temperature using a three-electrode cell. For comparison, HER catalytic measurement using $MoSe_2$, Pt and bare carbon have been conducted in the same conditions. Fig. 5A shows the polarization curves of the current density (*j*) *versus* the potential of the pure $MoSe_2$ and porous $MoSe_2$ synthesis, bare carbon and commercial Pt catalysts. Toward the negative potential direction, cathodic waves rise due to the electrocatalytic reduction of proton to H_2. For porous rose-like microspheres, onset overpotential of ~150 mV *vs.* RHE is recorded, corresponding to a small HER overpotential of ~300 mV for 6 mA cm^{-2} current density. However, pure $MoSe_2$ exhibits a clear inferior electrocatalytic activity compared to $MoSe_2$ rose-like microspheres. It is worth noting that monolayer flakes are significantly worse with an onset overpotential about −400 mV. We assume that the severe aggregation of monolayer flakes during electrocatalysis leads to the diminished surface areas and thus the poor HER performance. In this work the electrochemical performance of $MoSe_2$@Cu_2Se composite was not studied. This is due to Cu_2Se is able to oxidize in the potential range for HER study. So it can affect HER results. In addition, the distinguished catalytic performance of 3D porous structure of $MoSe_2$ is also indicated by the exceptionally low Tafel slope of ~56 mV per decade (Fig. 5B). In comparison with the 3D porous structure, higher Tafel slops of $MoSe_2$ compacted spheres (pure $MoSe_2$) was measured as ~71 mV per decade. We attribute these merits to the 3D porous structures of $MoSe_2$ rose-like microspheres which retain excellent structure rigidity and possess more catalytic sites during electrocatalysis. In the present work, the Tafel slope is 56 mV per decade for the porous $MoSe_2$ (rose-like structure), illustrating the Heyrovsky reaction plays a dominant role in determining the HER rate of this catalyst material. The Tafel slope in this work is indeed close to the values of 3D MoS_2/$MoSe_2$ nanosheet-graphene networks (61 mV per decade),[16] MoS_2/$MoSe_2$ host lattice (50–60 mV per decade)[21] $MoSe_2$/carbon fiber aerogel hybrids (62 mV per decade)[22] and compositing $MoSe_2$ on MoS_2 (65 mV per decade).[23]

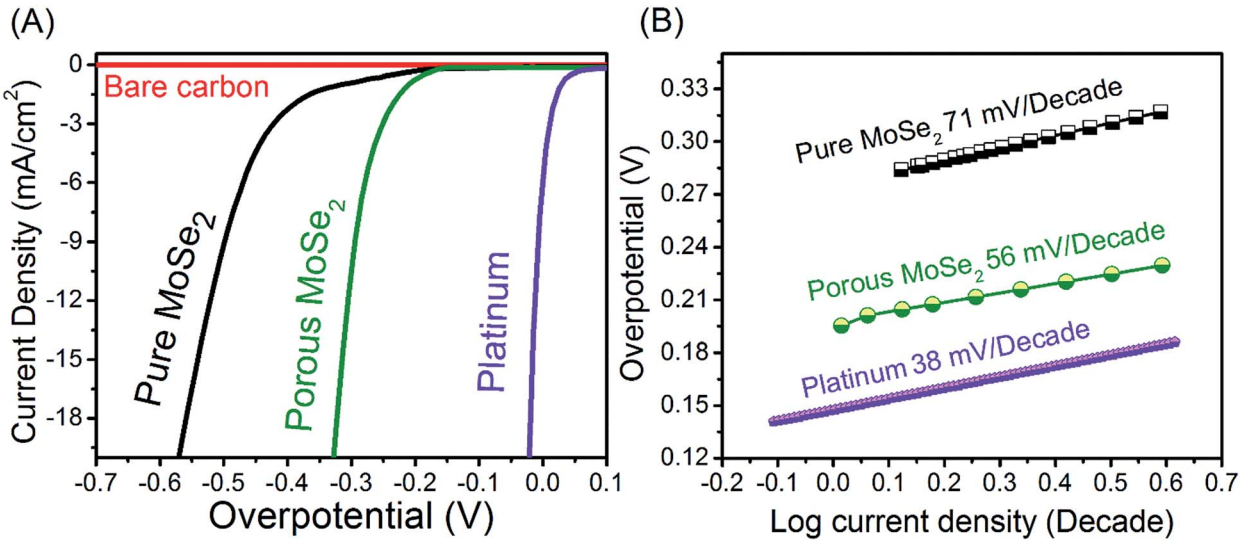

Fig. 5 Electrochemical measurements of $MoSe_2$ products. (A) Polarization curves and (B) corresponding Tafel plots obtained from the polarization curve of $MoSe_2$ porous microspheres in 0.5 M H_2SO_4 along with the bare carbon, pure $MoSe_2$ and platinum electrodes.

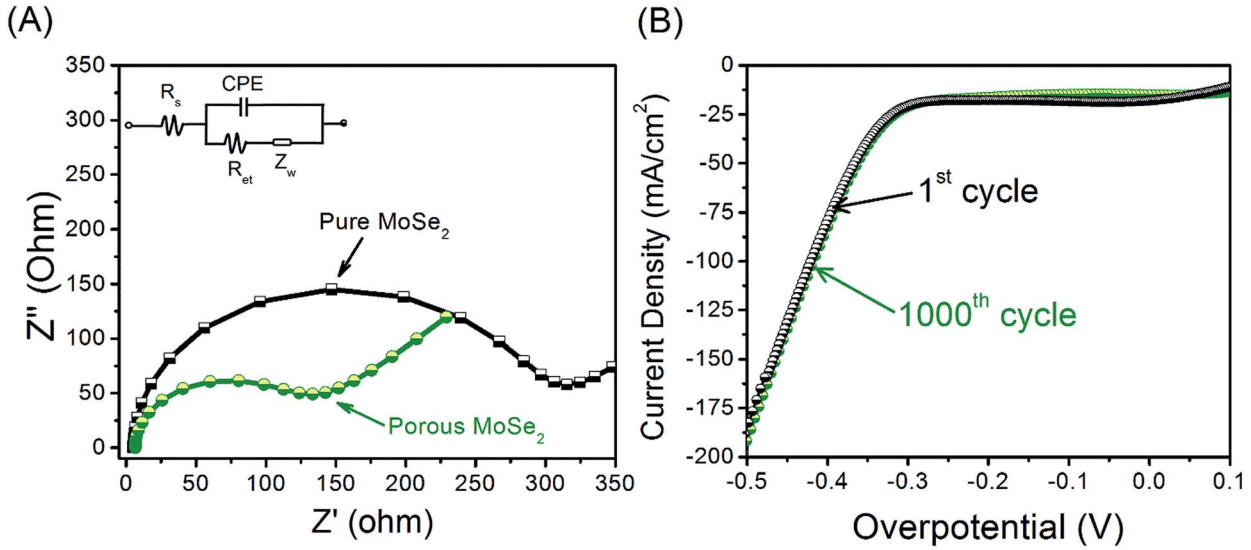

Fig. 6 (A) EIS Nyquist plots of pure $MoSe_2$ and porous $MoSe_2$. (B) Polarization curves of $MoSe_2$ porous microsphere catalyst before and after 1000 potential cycles in 0.5 M H_2SO_4.

Impedance spectroscopy (Fig. 6A) revealed that the pure $MoSe_2$ films themselves contributed significantly to the series resistance in addition to the substrate and solution resistances. Consequently, this may contribute to the observed trends in turnover frequency. The high degree of resistance from the pure $MoSe_2$ is not surprising, given that $MoSe_2$ possesses semiconducting as well as anisotropic charge transport properties. However, the charge transfer resistance of the porous $MoSe_2$ was much smaller. The material showed a charge transfer resistance of about 150 Ω. These results suggest that the conductivity of the porous $MoSe_2$ is much higher than that of pure $MoSe_2$, which indicates a much faster electron transfer process during electrochemical reaction. Other than high electrocatalytic activity, good durability is another important criterion in the selection of electrocatalysts. Here, $MoSe_2$ porous microsphere catalyst was continuously cycled for 1000 times in 0.5 M H_2SO_4. The polarization curves before and after 1000 cycles were compared as shown in Fig. 6B. Little HER activity loss is discernible, indicating that the 3D porous structure of $MoSe_2$ rose-like microspheres is highly stable and no significant electrocatalytic active sites were lost during the cycles.

Conclusions

We have demonstrated a simple and rational method to provide a significant enhancement of the electrocatalytic performance of porous rose-like $MoSe_2$ structure by a combination of hydrothermal and chemical etching methods. This new approach leads to favorable kinetics, metallic conductivity, and proliferation of active sites in a unique 3D architecture of 2H-$MoSe_2$. Benefiting from the 3D porous structures, the electrocatalytic profiles of the $MoSe_2$ rose-like microspheres as a catalyst for hydrogen evolution is evaluated, of which the result proves the excellent HER catalytic performance and good durability of 3D porous microspheres $MoSe_2$. We expect that this facile methodology could be expanded to prepare more 3D porous structures comprising their monolayered units, which will open new opportunities in exploring their undiscovered properties and applications.

Conflicts of interest

There are no conflicts to declare.

Acknowledgements

This work was supported through funding from the Natural Science and Engineering Research Council of Canada (NSERC), the Canada Research Chairs program (CRC) and Canada Foundation for Innovation. We acknowledge all the characterization centers including NanoQAM, Le Centre de Caractérisation Microscopique des Matériaux (CM^2) and Laboratoire de Caractérisation des Matériaux (LCM). We also thank Pr Daniel Belanger (UQAM) for the discussion about the electrochemical measurements.

References

1 L. Schlapbach and A. Zuttel, *Nature*, 2001, **414**(6861), 353–358.
2 J. A. Turner, *Science*, 2004, **305**(5686), 972–974.
3 M. S. Dresselhaus and I. L. Thomas, *Nature*, 2001, **414**(6861), 332–337.
4 N. S. Lewis and D. G. Nocera, *Proc. Natl. Acad. Sci. U. S. A.*, 2006, **103**(43), 15729–15735.
5 J. Greeley, T. F. Jaramillo, J. Bonde, I. Chorkendorff and J. K. Norskov, *Nat. Mater.*, 2006, **5**(11), 909–913.
6 M. Wang, L. Chen and L. Sun, *Energy Environ. Sci.*, 2012, **5**(5), 6763–6778.
7 V. W.-h. Lau, A. F. Masters, A. M. Bond and T. Maschmeyer, *Chem.–Eur. J.*, 2012, **18**(26), 8230–8239.

8 K. Rakstys, A. Abate, M. I. Dar, P. Gao, V. Jankauskas, G. Jacopin, E. Kamarauskas, S. Kazim, S. Ahmad, M. Grätzel and M. K. Nazeeruddin, *J. Am. Chem. Soc.*, 2015, **137**(51), 16172–16178.
9 Y. Zheng, Y. Jiao, M. Jaroniec and S. Z. Qiao, *Angew. Chem.*, 2015, **54**(1), 52–65.
10 M. Chhowalla, Z. Liu and H. Zhang, *Chem. Soc. Rev.*, 2015, **44**(9), 2584–2586.
11 S. Mao, Z. Wen, S. Ci, X. Guo, K. Ostrikov and J. Chen, *Small*, 2015, **11**(4), 414–419.
12 Y. Zhang, Q. Gong, L. Li, H. Yang, Y. Li and Q. Wang, *Nano Res.*, 2015, **8**(4), 1108–1115.
13 X. Hu, W. Zhang, X. Liu, Y. Mei and Y. Huang, *Chem. Soc. Rev.*, 2015, **44**(8), 2376–2404.
14 J. C. Shaw, H. Zhou, Y. Chen, N. O. Weiss, Y. Liu, Y. Huang and X. Duan, *Nano Res.*, 2014, **7**(4), 511–517.
15 L. Jia, X. Sun, Y. Jiang, S. Yu and C. Wang, *Adv. Funct. Mater.*, 2015, **25**(12), 1814–1820.
16 S. Xu, Z. Lei and P. Wu, *J. Mater. Chem. A*, 2015, **3**(31), 16337–16347.
17 H. Huang, L. Chen, C. Liu, X. Liu, S. Fang, W. Liu and Y. Liu, *J. Mater. Chem. A*, 2016, **4**(38), 14577–14585.
18 D. Kong, H. Wang, J. J. Cha, M. Pasta, K. J. Koski, J. Yao and Y. Cui, *Nano Lett.*, 2013, **13**(3), 1341–1347.
19 F. Lin, G.-Q. Bian, Z.-X. Lei, Z.-J. Lu and J. Dai, *Solid State Sci.*, 2009, **11**(5), 972–975.
20 C. Dai, E. Qing, Y. Li, Z. Zhou, C. Yang, X. Tian and Y. Wang, *Nanoscale*, 2015, **7**(47), 19970–19976.
21 V. Kiran, D. Mukherjee, R. N. Jenjeti and S. Sampath, *Nanoscale*, 2014, **6**(21), 12856–12863.
22 Y. Zhang, L. Zuo, L. Zhang, Y. Huang, H. Lu, W. Fan and T. Liu, *ACS Appl. Mater. Interfaces*, 2016, **8**(11), 7077–7085.
23 X. Lei, K. Yu, H. Li, Z. Tang and Z. Zhu, *J. Phys. Chem. C*, 2016, **120**(28), 15096–15104.